



# CHORUS

This is the accepted manuscript made available via CHORUS. The article has been published as:

## Determining whether metals nucleate homogeneously on graphite: A case study with copper

David Appy, Huaping Lei, Yong Han, Cai-Zhuang Wang, Michael C. Tringides, Dahai Shao, Emma J. Kwolek, J. W. Evans, and P. A. Thiel

Phys. Rev. B **90**, 195406 — Published 5 November 2014

DOI: [10.1103/PhysRevB.90.195406](https://doi.org/10.1103/PhysRevB.90.195406)

## Determining Whether Metals Nucleate Homogeneously on Graphite: A Case Study with Copper

David Appy,<sup>a,b</sup> Huaping Lei,<sup>a,c,e</sup> Yong Han,<sup>a,c</sup> Cai-Zhuang Wang,<sup>a</sup> Michael C. Tringides,<sup>a,c</sup> Dahai Shao,<sup>a,b</sup> Emma J. Kwolek,<sup>b</sup> J. W. Evans,<sup>a,c</sup> and P. A. Thiel<sup>a,b,d</sup>

<sup>a</sup>The Ames Laboratory, Ames, Iowa 50011 USA

<sup>b</sup>Department of Chemistry, Iowa State University, Ames, Iowa 50011 USA

<sup>c</sup>Department of Physics & Astronomy, Iowa State University, Ames, Iowa 50011 USA

<sup>d</sup>Department of Materials Science & Engineering, Iowa State University, Ames, Iowa 50011 USA

<sup>e</sup>Present address: Key Laboratory of Materials Physics, Institute of Solid State Physics, CAS, China

### **Abstract.**

We observe that Cu clusters grow on surface terraces of graphite as a result of physical vapor deposition in ultrahigh vacuum. We show that the observation is incompatible with a variety of models incorporating homogeneous nucleation and high-level calculations of atomic-scale energetics. An alternative explanation, ion-mediated heterogeneous nucleation, is proposed and validated, both with theory and experiment. This serves as a case study in identifying when and whether the simple, common observation of metal clusters on carbon-rich surfaces can be interpreted in terms of homogeneous nucleation. We describe a general approach for making system-specific and laboratory-specific predictions.

### **Introduction.**

The conditions under which solids grow on solid surfaces determine the structure, properties, and distribution of the grown material. One of the simplest—and most informative—growth scenarios is that in which single atoms impinge on a solid surface, then diffuse randomly and aggregate into clusters. This situation is informative because there can be a direct relationship between clusters' characteristics (e.g. number density and size distribution) and the energetics of individual processes (e.g. diffusion of atoms and cluster nucleation). However, there is a basic condition for applying this relationship: Nucleation and growth must occur on homogeneous (defect-free) surface regions. Usually, the experimental observation of clusters on low-index surface terraces is taken to be a strong indication that this condition is met.

A timely example of solid-on-solid growth is that of metals on carbon-based solids, especially on graphene and graphite. This type of combination is important for major energy-related technologies involving catalysis [1] and electrochemistry [2, 3], and also for the exploitation of carbon-based solids in magnetic or electronic devices [4, 5]. There have been many studies of model systems, especially studies of transition metals on graphite. [6] In these studies, it has been very common to observe clusters of metals on the (0001) terraces of graphite [6]. However, only rarely have the clusters' characteristics been analyzed in relation to the mechanism or energetics of homogeneous nucleation and

growth described above [7, 8]. Those few analyses have been hampered by the unavailability of theory at a level sufficient to predict the basic energetics for metals on graphite, i.e. sufficient to test the interpretation of the experimental results.

In this paper, we report experimental observations of Cu clusters grown on graphite(0001) terraces, and ask whether it is reasonable to interpret our observations in terms of homogeneous nucleation and growth. This task is made possible by concurrent high-level calculations of energetic parameters for metals on graphite using density functional theory (DFT) with van der Waals corrections, together with Kinetic Monte Carlo (KMC) simulations adapted to diverse nucleation and growth models. We show that it is impossible that nucleation is homogenous in this case. We demonstrate conclusively that a different mechanism (heterogeneous nucleation) is operative. Most importantly, we comment on the conditions under which homogeneous nucleation and growth can generally be expected for metals on graphite, an approach that may also prove useful for metals on other carbon-rich surfaces.

## **2. Details of the approach.**

### **2a. Experimental details.**

Experimentally, we use scanning tunneling microscopy (STM) to characterize carbon surfaces before and after deposition of Cu in ultrahigh vacuum (UHV) via physical vapor deposition (PVD). PVD is commonly used to produce single metal atoms that impinge on the surface, hence achieving the first step in the simple growth scenario described above. The evaporator is a Mantis QUAD-EV-C Mini e-beam Evaporator. The crucible is made of molybdenum, with a pyrolytic boron nitride (PBN) liner. The crucible is held at +2 kV with respect to an electron filament mounted parallel to and near the top of the evaporation target.

HOPG samples (ZYA grade) are cleaved in air with tape and transferred into UHV, then heated to 800 K. During subsequent Cu deposition, the HOPG sample is at 300 K. Cu coverage is calculated from STM images, but only for the HOPG terraces, i.e. Cu at step edges is not included. Because lateral dimensions of the small Cu islands are unreliable due to convolution between the island and the STM tip, island volumes are calculated from island heights, assuming the shapes to be hemispherical. (Other authors [8, 9] have estimated that metal islands on HOPG have actual widths that are only 50-60% of the appearance in STM images, for island diameters around 10 nm.)

Tunneling parameters for imaging the clean HOPG surface are in the range 0.05 to 1.00 V tip bias and 0.1 to 1.0 nA current. Optimal tunneling parameters for imaging the 3D Cu islands on the graphite surface are different. Islands are easily displaced by the tip. This effect is somewhat mitigated by using tip bias of -0.8 to -2.5 V, current of 0.02 to 0.3 nA, and a scan speed of 800 to 1200 nm/s (for 250 nm x 250 nm images). Faster scanning causes many islands to be displaced, and often causes loss of tunneling altogether. Slower scanning is not markedly advantageous.

### **2. Computational Details: DFT.**

First-principles energy calculations with non-local vdW correction are performed based on density functional theory (DFT) using VASP 5.3 [10]. The exchange and correlation energy functional adapts the opt-PBE scheme developed by Klimes et al. [11-13]. This functional has been verified to describe accurately the energy and other

properties of graphite and metals [12, 14]. The electron-ion interaction is described by the projector augmented wave method [15]. The energy cutoff for the plane wave basis set used in the calculation is 400 eV. The fundamental properties of graphite (in A-B stacking) calculated from this set up are: 0.246 nm for the lattice constant; 0.336 nm and -69 meV/atom for the interlayer separation and its binding energy; 0.112 J/m<sup>2</sup> for graphite (0001) surface energy; and 36.5 GPa for the elastic constant  $C_{33}$ . These values are in good agreement with the experimental values of 0.246 nm, 0.333 nm,  $-52 \pm 2$  meV/atom, 0.1-0.2 J/m<sup>2</sup> and  $36 \pm 1$  GPa, respectively. The calculated lattice constants and cohesive energies of fcc Cu are 0.363 nm and 3.74 eV/atom respectively, also in good agreement with experimental data of 0.361 nm and 3.49 eV/atom, respectively [16-19].

In the calculation for Cu adsorption on graphite, the graphite substrate is modeled by a slab with a 6x6 unit cell in the  $xy$  plane and 4 layers along the (0001) direction, plus enough vacuum (1.57 nm) to avoid interaction between the slab and its images under the periodic boundary condition. A  $\Gamma$ -centered  $k$ -point grid of 3x3x1 is used in the calculation. In the calculation of Cu adsorption on the zigzag edge, i.e. the (1-210) face, the supercell is enlarged to 4x4 in the  $xy$  plane and to 6 layers along the  $z$  axis. The top layer is cut by half along the [1-210] direction to simulate the zigzag edge configuration. The  $k$ -point grid is 6x2x1. For the armchair edge of graphite, i.e. the (10-10) face, the supercell in the  $xy$  plane is 8x2 with 6 layers in the  $z$ -direction. The  $\Gamma$ -centered  $k$ -point grid is 2x6x1. Similar to the zigzag edge construction, the top layer is cut by half along the [10-10] direction to simulate the armchair edge configuration. Both types of supercells for the edge adsorption contain 352 atoms. During geometric optimization, the bottom 5 layers are fixed to their bulk positions, while the carbon atoms in the top layer and metal adatom are relaxed fully with a force tolerance of 0.01 eV/Å.

## 2c. Kinetic Monte Carlo simulations.

Our homogeneous stochastic nucleation models involve random deposition onto a periodic lattice of adsorption sites at rate  $F$ , diffusive hopping between neighboring sites at rate  $h$ , and irreversible nucleation (when two diffusing atoms meet) and aggregation with existing islands. In our ‘‘point island’’ models [20], nanoclusters occupy a single site but carry a size label,  $s$ . In the basic model, a diffusing adatom on a site adjacent to a nanocluster (or other atom) hops onto the same site at rate  $h$ , where it is irreversibly incorporated, hence increasing the island size by +1. Model modifications include: (i) incorporating a reduced rate (corresponding to an extra barrier) for this last hop leading to nucleation or aggregation; and (ii) blocking island growth above a threshold size,  $s^*$ .

Efficient Kinetic Monte Carlo simulation is implemented on a finite periodic array of  $M_{tot} \sim 10^6$ - $10^7$  adsorption sites with periodic boundary conditions using a Bortz-Kalos-Lebowitz algorithm [21]. This algorithm maintains a list of the  $M_{hop}$  diffusing adatoms and their locations. In the basic model, the total rate for deposition or diffusion events is then  $R_{tot} = FM_{tot} + zhM_{hop}$ , where  $z$  is the coordination number for adsorption sites (i.e., the number of directions to hop). At each simulation step, one selects deposition with probability,  $P_{dep} = FM_{tot}/R_{tot}$ , and hopping with probability  $P_{hop} = zhM_{hop}/R_{tot} = 1 - P_{dep}$ . For deposition the adsorption site is randomly selected, and for hopping the direction is randomly selected. After each deposition event creating a new diffusing adatom, one adds an entry to the above-mentioned list. After each nucleation or aggregation event, one removes an entry from the list, and updates nanocluster sizes.

With this algorithm, we efficiently simulate for high  $h/F$ -ratios appropriate for the Cu/HOPG system up to  $\sim 10^{15}$  (well beyond previous simulations [20, 22, 23]).

### **3. Experimental and Computational Results.**

Three-dimensional (3D) Cu islands form on terraces over a wide range of Cu coverage. Fig. 1 shows images for coverages spanning 0.04 to 0.21 ML. Islands are visible on terraces even at the lowest coverage. Steps are covered well before terraces. The average number density,  $N$ , of Cu clusters on terraces increases roughly linearly with Cu coverage through the first Cu ML, then it plateaus as the amount of exposed HOPG becomes smaller, as shown in Fig. 2(a). Our discussion will focus on behavior at or below 0.3 ML because there, the exposed HOPG clearly plays a major role in adsorption and nucleation of incident Cu atoms (accounting for at least 85% of the exposed terrace area). In this regime, the cluster/island size distribution (ISD) (i.e. the density  $N_s$  of Cu clusters with  $s$  atoms) decays monotonically, as shown in Fig. 2(b).

DFT provides basic energetic insights. (See SI for details.) It is noteworthy that our calculations incorporate the dispersion forces that bind the carbon sheets in graphite. DFT shows that a Cu atom adsorbs atop a C atom with no C atom in the layer beneath (the graphite  $\beta$  site [6]), and the adsorption energy ( $E_{ads}$ ) is 0.589 eV. A Cu atom diffuses between  $\beta$  sites along C-C bonds, with an associated energy barrier ( $E_{diff}$ ) of 0.020 eV. Adsorption of Cu at the steps of basal planes of graphite is far stronger than on terraces—4.76 eV on the (1-210) step, and 3.38 eV on the (10-10) step. This strong adsorption at steps, combined with the low  $E_{diff}$  on terraces, explains the observation (above) that Cu accumulates preferentially at step edges. In addition, the observed 3D cluster morphology is consistent with DFT, where clusters of 2-4 Cu atoms always relax to 3D configurations, leaving only 1 or 2 Cu atoms interacting with the graphite(0001) surface. In summary, both preferential step decoration and 3D cluster morphology are supported by theory.

The information from both DFT and experiment is used to build realistic models for KMC simulations, as follows. The small footprint of the 3D Cu islands on the surface (cf. Fig. 1) justifies the use of efficient “point island” models as described in Section 2.3. These models all include deposition at rate  $F = 4 \times 10^{-4}$  ML/s (consistent with experiment) and diffusion at rate  $D = D_0 \exp(-E_{diff}/kT)$  (in  $\text{nm}^2/\text{s}$ ) between  $\beta$  sites. We choose a typical value of  $D_0/\Omega = 10^{12.5} \text{ s}^{-1}$  where  $\Omega = 0.052 \text{ nm}^2$  is the unit cell area. A critical size,  $i$ , is defined such that islands with  $s > i$  are stable. Desorption can be ignored, since the DFT values  $E_{ads} = 0.589 \text{ eV}$  and  $E_{diff} = 0.020 \text{ eV}$  mean that a Cu atom at room temperature diffuses a net distance of about 20  $\mu\text{m}$  before desorbing—much farther than the typical terrace width of 1  $\mu\text{m}$ .

Within this framework, our goal is to find (if possible) a realistic model for which KMC simulation reproduces the experimental behaviors of  $N$  and  $s$  in Fig. 2. The simplest model, denoted Model 1, is homogeneous nucleation with  $i = 1$ . Using  $E_{diff} = 0.020 \text{ eV}$  from DFT, KMC shows that  $N = 8 \times 10^{-5} \text{ nm}^{-2}$  at 0.1 ML and room temperature. This is well below the corresponding experimental value of  $1 \times 10^{-3} \text{ nm}^{-2}$  at 0.1 ML from Fig. 2a. In fact, to reproduce the experimental value of  $N$ , a value of  $E_{diff} = 0.21 \text{ eV}$  would be necessary—a factor of 10 higher than the DFT value. Model 1 also fails to match the experimental data by exhibiting non-linear  $N(\theta)$  (specifically,  $N \propto \theta^{1/3}$ ) and a monomodal

ISD. In short, Model 1 disagrees with experiment on all counts. Introducing  $i > 1$  or Cu cluster diffusion only serves to lower the theoretical value of  $N$  and thus to exacerbate the discrepancy.

We have used KMC to assess a number of variations of Model 1. We call these collectively Model 2. One such variation includes an extra barrier for aggregation and nucleation, which would reflect short-range adatom repulsions. This boosts  $N$  to match experiment while retaining  $E_{diff} = 0.020$  eV. However, a large nearest-neighbor barrier of 0.23 eV is needed, whereas DFT indicates that the repulsive barrier does not exceed 0.02 eV. Another variation includes repression of island growth above a threshold size,  $s^*$ , which could have its physical origin in charge or strain accumulation in the growing cluster. In another variation, nucleation is initiated via an analog of a place-exchange event, i.e. a diffusing Cu atom reacts with the graphite substrate and subsequently serves as a fixed nucleation site. However, none of these models reproduces all three aspects of the experimental data—the magnitude of  $N$ , linear  $N(\theta)$ , and monotonically decreasing ISD—at least not for  $E_{diff} \approx 0.020$  eV and realistic  $F$ . In short, no homogeneous nucleation model reproduces the experimental data.

We thus turn to the possibility of heterogeneous nucleation. Conventionally, heterogeneous nucleation is controlled by pre-existing defects. It is well known that small defects—probably carbon vacancies—exist on HOPG surfaces, but their reported densities are typically much lower than our observed  $N$ , ranging from  $1 \times 10^{-8}$  to  $8 \times 10^{-5}$   $\text{nm}^{-2}$ . We have examined our HOPG surfaces carefully using STM, and estimate that the upper bound on the defect density is  $1 \times 10^{-5}$   $\text{nm}^{-2}$ . We thus rule out the possibility that Cu cluster nucleation on terraces is primarily due to pre-existing (intrinsic) defects.

Another possibility is suggested by experiment. Close examination of the STM images reveals that Cu clusters are sometimes displaced by the scanning tip, and they consistently leave behind a small residue, as shown in Fig. 3. This raises the possibility that the residue is the original nucleation site. If the residue does not reflect an intrinsic defect, perhaps it is an *extrinsic* defect—a defect induced by the deposition process itself.

It is known that metal flux emitted from a hot source always contains a fraction of ions, given by the Saha-Langmuir equation. In an e-beam evaporator, there can be additional ionization by electrons accelerated from the emission filament toward the crucible. Other groups have shown that metal ions generated in an e-beam evaporator can affect film structure, and can induce surface alloying on *metal* surfaces. However, the effect of ions is usually overlooked or discounted in physical vapor deposition.

Fig. 4a shows the results of experiments in which Cu was deposited for 10 s with the e-beam voltage and filament current both on, as normal. Cu clusters are present on the step *and* the terraces. In contrast, Fig. 4b shows the result when both voltage and current are off, starting at the same initial conditions. (Of course, the crucible cools during the 10 s period, but we have measured the consequent flux drop using a Cu(100) substrate in place of HOPG, which indicates that the drop is only  $26 \pm 5\%$ ). In this experiment, clusters decorate only the step edge and the terraces remain pristine. The result is entirely reproducible at different Cu fluxes and different Cu coverages. Clusters form on terraces only if *both* the high voltage and filament current are on. We conclude that the damaging Cu ions are generated by the e-beam heating configuration, and that clusters nucleate on terraces at points where these Cu ions damage the carbon substrate. In that case it is

likely that the residue left by a 3D cluster is a small raft of Cu atoms in and around a C vacancy.

To test whether this concept is compatible with the experimental  $N(\theta)$  and ISD, we have developed Model 3, a heterogeneous nucleation model in which a fraction,  $p$ , of deposited Cu atoms stick where they land and facilitate island nucleation. Choosing  $p = 5 \times 10^{-4}$  ensures that the density of islands nucleated by defects at 0.1 ML will be  $5 \times 10^5$ /site, or  $1 \times 10^{-3} \text{ nm}^{-2}$  (the experimental value). Islands can still nucleate homogeneously, but they are in the minority. The simulation results for point islands show the expected initial near-linear increase in  $N(\theta)$  for this model, and also a monotonically decreasing ISD, both compatible with experiment. The simulation results are shown in Fig. 2.

To test the model even further, we develop an analytic theory to capture higher- $\theta$  behavior. Since only ions depositing directly on HOPG (versus on existing Cu islands) can nucleate new islands, the nucleation rate is given by  $dN/d\theta = (p/\Omega) A(\theta)$ , where  $A(\theta)$  is the fraction of exposed HOPG. In a simplified picture where 3D Cu islands grow at constant rate after nucleation, their radius grows like the 1/3 power of the time after nucleation, up until coalescence. Given this form of the radial growth rate, and noting the constant rate of nucleation on exposed HOPG, one can adapt JMAK theory,<sup>19</sup> which accounts for coalescence effects, to show that  $A(\theta) = \exp[-c \theta^{5/3}]$ . Setting  $c = 0.75$  to recover the experimental  $A$ -value at 1 ML, yields the dotted curve for  $N(\theta)$  shown in Fig. 2(a), matching well the experimental data at high  $\theta$  and validating the model of heterogeneous nucleation further.

In addition to island densities and size distributions, our simulations also generate the spatial distribution of islands on the surface. Fig. 5 shows examples of these spatial distributions for: (a) the classic irreversible nucleation model (with critical size  $i = 1$ ); (b) a refined model where there is a barrier for nucleation and aggregation so that the hop rate leading to nucleation or aggregation is 0.01 of the terrace hop rate; (c) the preferred model where random nucleation is initiated by a deposition of a small fraction of ions in the deposition. For optimal comparison, in all cases, we adjust the simulation parameters to produce roughly the same number ( $\sim 210$ ) of islands in the  $2000 \times 2000$  site simulation system, i.e., an island density of  $N_{\text{isl}} \approx 5 \times 10^{-5}$  per site. Clearly the island distribution in the classic nucleation model (a) is non-random, exhibiting anti-clustering (the population of nearby islands is smaller than for a random distribution). The distribution for model (c) is perfectly random. The distribution for model (b) is more random than (a), a natural consequence of the barrier for nucleation.

#### **4. Discussion.**

We now put these results and insights into broader context. First, in the literature, there is ample evidence that *deliberate* ion damage of graphite can enhance nucleation of metal atoms on graphite terraces. This ion damage has been induced (most often) by noble gas sputtering prior to metal deposition. Our work is different, in that ion damage occurs under conditions normally assumed to be benign. Indeed, inadvertent metal ion damage may be responsible for some prior reports of metal clusters on graphite terraces. For example, two separate groups studied Ag deposited via PVD on HOPG, using STM. One group saw clusters on terraces, using an e-beam evaporator, whereas the other saw no clusters, using a resistively-heated evaporator. There were also other differences in

experimental conditions, but our results point to one possible cause of the discrepant observations.

The most important general question is this: When is it reasonable to attribute transition metal clusters on graphite(0001) terraces to homogeneous nucleation? It is impossible to frame a simple quantitative answer because there are many factors that can vary from study to study, especially the experimental ability to detect clusters (which depends on the technique, plus cluster morphology and size) and the experimental conditions (including  $F$ ,  $T$ , and  $\theta$ ). We can, however, compare the value of  $N$  predicted for different metals, for simple homogeneous nucleation under a fixed set of conditions. We choose  $F$  and  $T$  to be the same as in this study, and set  $\theta = 0.10$  ML and  $i = 1$ . The comparison is then controlled by  $E_{diff}$ , which has been determined from DFT for only a few metals on graphite (Cr, Pt, Cu, Ag, and Au), the extremes being Pt ( $E_{diff} = 0.161$  eV) and Au ( $E_{diff} = 0.006$  eV). Model 1 yields  $N = 5 \times 10^{-4} \text{ nm}^{-2}$  for Pt, and  $7 \times 10^{-5} \text{ nm}^{-2}$  for Au. Thus, predicted values of  $N$  for metals in this group span less than an order of magnitude, with Cu intermediate. If simple homogeneous nucleation is observed for any of these metals,  $N$  should fall in this rather narrow range, under the specified conditions.

What about other conditions?  $N$  increases (weakly) with increasing  $F$  or  $\theta$ , for instance, making observation of clusters on terraces more likely at higher  $F$  or  $\theta$ . Predictions of  $N$  can be translated to different conditions using well-known scaling relationships applicable to Model 1. If a measured  $N$  is significantly *larger* than predicted, then the picture of homogeneous nucleation must be modified strongly (e.g. Model 2), or heterogeneous nucleation is involved (e.g. Model 3), but in either case, simple homogeneous nucleation (Model 1) does not apply. If a measured value of  $N$  is significantly *smaller* than predicted, then Model 1 is viable because  $N$  can be adjusted downward with  $i > 1$  and/or cluster diffusion. [An example of this may be Au on graphite, where  $N \approx 10^{-6} \text{ nm}^{-2}$  has been reported by several groups [7]. As in our study of Cu/HOPG, analyses of  $N(\theta)$  and the ISD can be powerful tools for identifying the correct model. We conclude that metal cluster growth on smooth graphite terraces—a simple and common observation in the literature [6]—must be interpreted with care, certainly for graphite and possibly for other carbon-rich surfaces as well.

#### **4. Summary.**

We have shown that homogeneous nucleation of Cu clusters on pristine graphite terraces is physically unreasonable, given the diffusion barrier calculated from DFT, under our particular set of experimental conditions ( $F$ ,  $T$ ,  $\theta$ ). The explanation for our experimental observation is, instead, ion-mediated nucleation in which the ions comprise a small fraction (about  $5 \times 10^{-4}$ ) of the total Cu flux. This case study demonstrates the importance and the method of testing, quantitatively, whether cluster densities observed experimentally are compatible with simple homogeneous nucleation. It is noteworthy that growth of metal clusters on graphite terraces is a common observation in the literature.

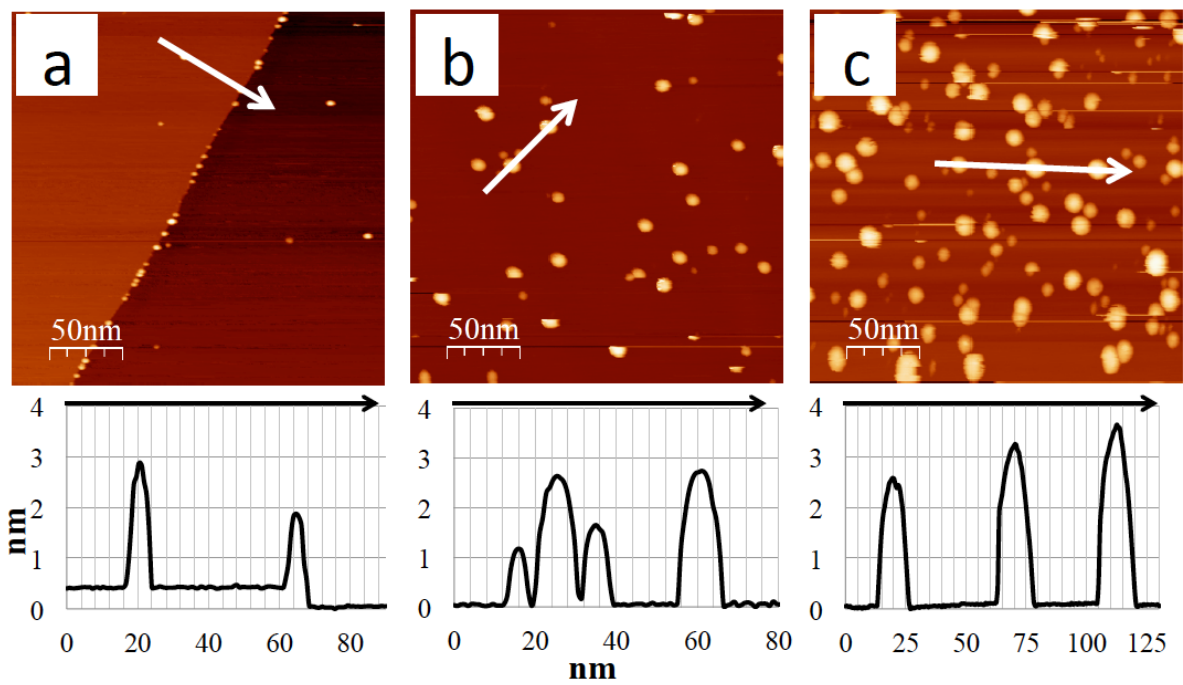
#### **Acknowledgements**

The experimental and DFT components of this work were supported by the Office of Science, Basic Energy Sciences, Materials Sciences and Engineering Division of the US Department of Energy (USDOE), under Contract No. DE-AC02-07CH11358 with the

US Department of Energy. YH and JWE were supported by NSF Grants CHE-1111500 for modeling and KMC simulation. We thank R. S. Houk, A. Schmid, and M. Schmid for useful insights, and J. Andereg for HOPG samples.

## **References**

1. F. Rodriguez-Reinoso, *Carbon*, **36** 159 (1998).
2. C.A. Bessel, K. Laubernds, N.M. Rodriguez, and R.T.K. Baker, *J. Phys. Chem. B*, **105** 11215 (2001).
3. J. Qiao, Y. Liu, F. Hong, and J. Zhang, *Chem. Soc. Rev.*, **43** 631 (2014).
4. X. Liu, C.-Z. Wang, M. Hupalo, H.-Q. Lin, K.-M. Ho, and M.C. Tringides, *Crystals*, **3** 79 (2013).
5. X. Liu, C.Z. Wang, M. Hupalo, W.C. Lu, M.C. Tringides, Y.X. Yao, and K.M. Ho, *Physical Chemistry Chemical Physics*, **14** 9157 (2012).
6. D. Appy, H. Lei, C.-Z. Wang, M.C. Tringides, D.-J. Liu, J.W. Evans, and P.A. Thiel, *Prog. Surf. Sci.*, **89** 219 (2014).
7. R. Anton and I. Schneiderreit, *Phys. Rev B*, **58** 13874 (1998).
8. H. Hövel, T. Becker, A. Bettac, B. Reihl, M. Tschudy, and E.J. Williams, *J. App. Phys.*, **81** 154 (1997).
9. I. Lopez-Salido, D.C. Lim, and Y.D. Kim, *Surf. Sci*, **588** 6 (2005).
10. G. Kresse and J. Furthmüller, *Comput. Mater. Sci.*, **6** 15 (1996).
11. J.P. Perdew, K. Burke, and M. Ernzerhof, *Phys. Rev. Lett.*, **77** 3865 (1996).
12. J. Klimes, D.R. Bowler, and A. Michaelides, *Phys. Rev B*, **83** 195131 (2011).
13. J. Klimes, D.R. Bowler, and A. Michaelides, *J. Phys.: Condens. Matter*, **22** 022201 (2010).
14. G. Graziano, J. Klimes, F. Fernandez-Alonso, and A. Michaelides, *J. Phys: Condens. Matter.*, **24** 424216 (2012).
15. P.E. Blöchl, *Phys. Rev. B*, **50** 17953 (1994).
16. D.R. Lide, Ed. *CRC Handbook of Chemistry and Physics*. 84th edition (2008) CRC Press: Boca Raton, Florida.
17. R. Zacharia, H. Ulbricht, and T. Hertel, *Phys. Rev. B*, **69** 155406 (2004).
18. N. Mounet and N. Marzari, *Phys. Rev. B*, **71** 205214 (2005).
19. N. Ooi, A. Rairkar, and J.B. Adams, *Carbon*, **44** 231, (2006).
20. M.C. Bartelt and J.W. Evans, *Phys. Rev. B*, **46** 12675 (1992).
21. A.B. Bortz, M.H. Kalos, and J.L. Lebowitz, *J. Comp. Phys.*, **22** 403 (1976).
22. M.C. Bartelt, J.B. Hannon, A.K. Schmid, C.R. Stoldt, and J.W. Evans, *Colloids and Surfaces A: Physicochemical and Engineering Aspects*, **165** 373-403 (2000).
23. J.W. Evans, P.A. Thiel, and M.C. Bartelt, *Surf. Sci. Rep.*, **61** 1 (2006).

**Figures and Captions**

**Fig. 1.** STM images of Cu clusters on HOPG terraces, 250 nm x 250 nm, -0.8V to -1.0V, 0.1 nA. (a) 0.003 ML; (b) 0.10 ML; (c) 0.21 ML.

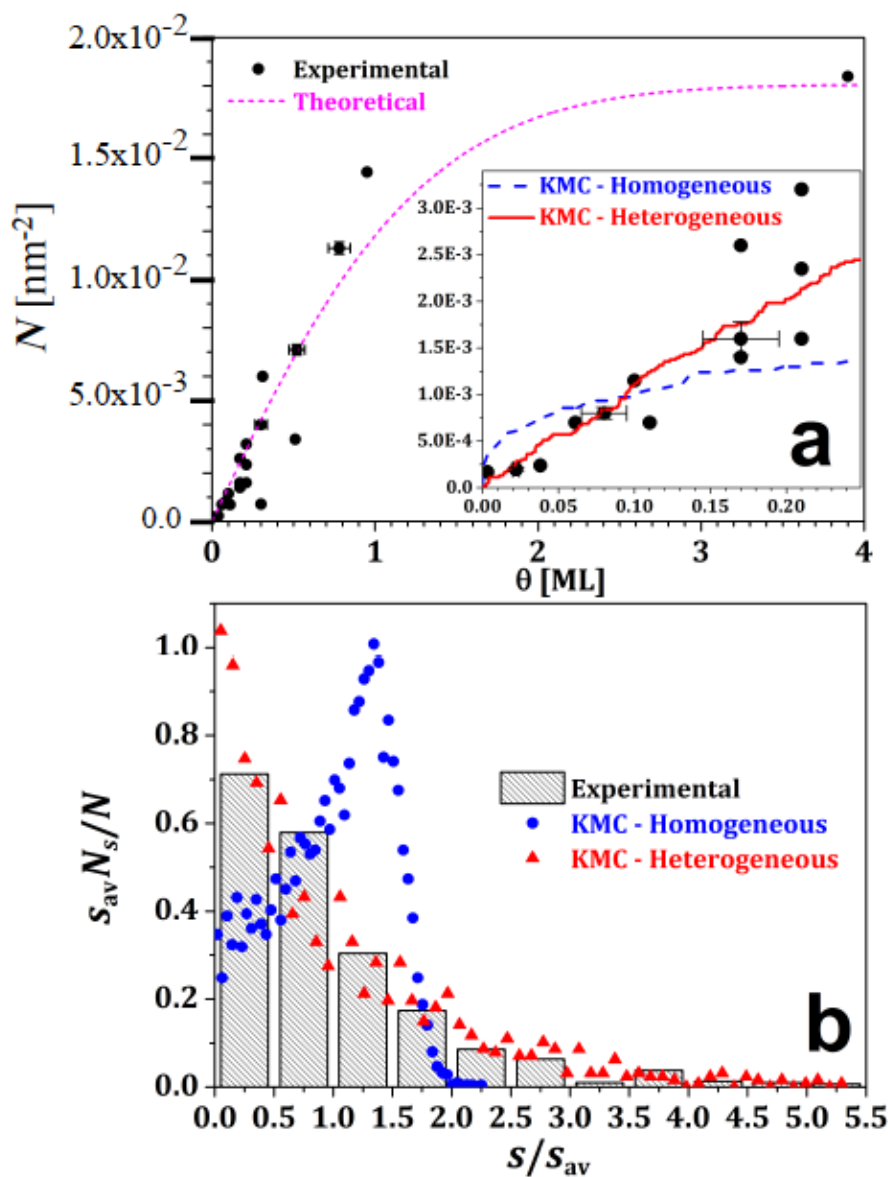


**Fig. 2.** (a)  $N$  vs. coverage ( $\theta$ ) for experiment (dots), and theory (dashed line). Inset: KMC results for homogeneous (dashed line) and heterogeneous (solid line) nucleation. Error bars reflect statistical uncertainty based on sample size. Ion flux variation is reflected in scatter. (b) Scaled ISD for 0.1 ML from experiment (bars, 632 islands total), and from KMC simulations for homogeneous (dotted line, 5164 islands) and heterogeneous (solid line, 1261 islands) nucleation.

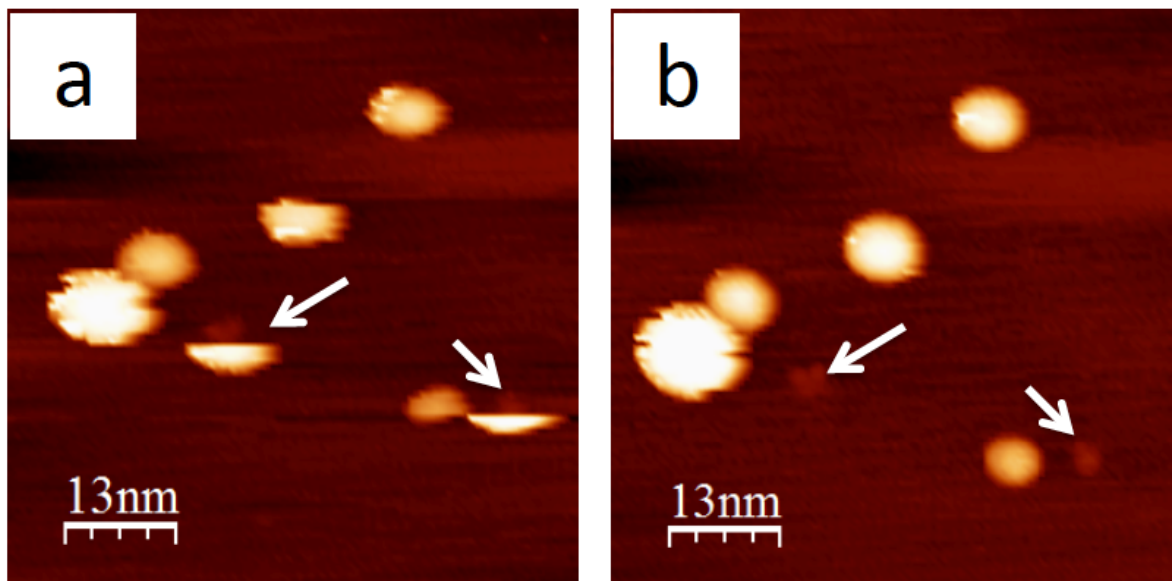


**Fig. 3.** Consecutive STM images, 67 nm x 67 nm, over the same area showing Cu islands removed by the STM tip. Conditions: 0.1 ML Cu, -0.8V, 0.1nA. (a) First scan, with sheared islands marked by arrows; (b) Second scan, arrows showing small residues where Cu islands were removed.

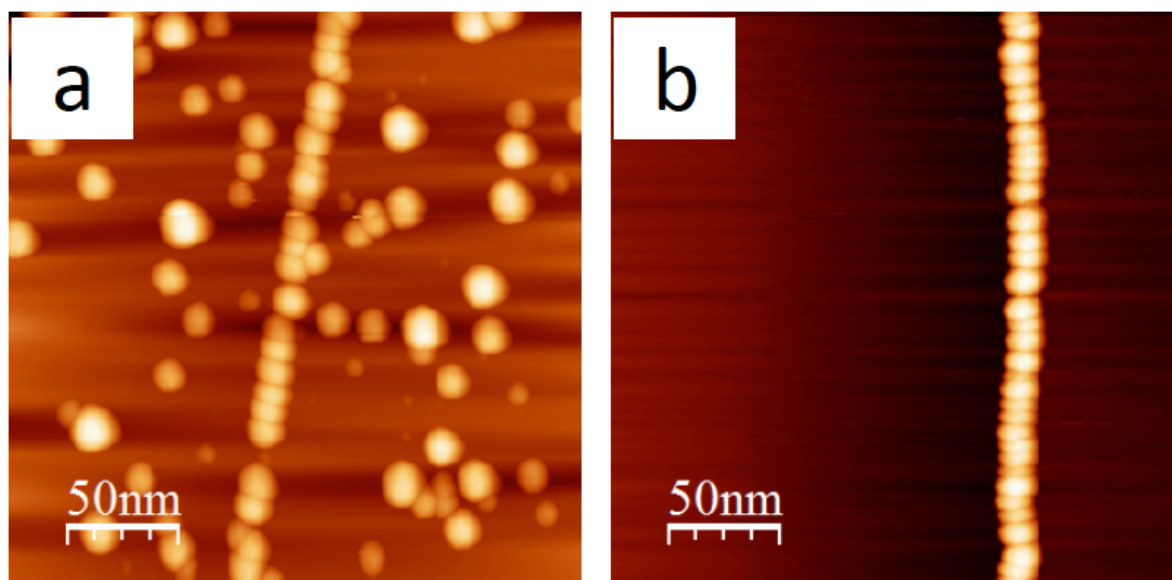


**Fig. 4.** Nucleation behavior on HOPG for Cu deposited using an e-beam heater. (a) Both crucible bias and filament on. (b) Bias and filament off.

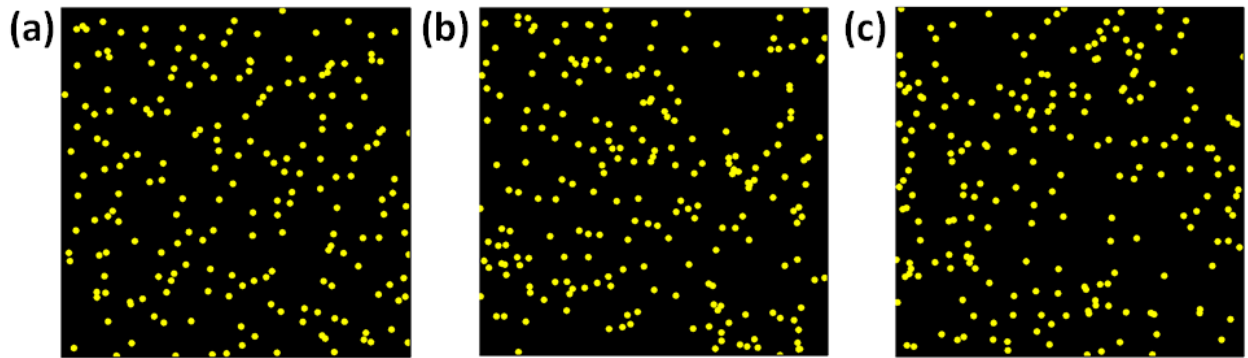


**Fig. 5.** Simulated island distributions in a  $2000 \times 200$  site system: (a) Model 1, classic irreversible homogeneous nucleation, showing 201 islands; (b) Model 2, refined homogeneous nucleation with a barrier for nucleation and aggregation, showing 217 islands; (c) Model 3, random defect-mediated nucleation, showing 209 islands.